KSCE Journal of Civil Engineering (2021) 25(3):757-767
DOI 10.1007/s12205-021-0263-y

pISSN 1226-7988, eISSN 1976-3808
www.springer.com/12205

Geotechnical Engineering

# Post Buckling Behavior of Slender Piles Partially Embedded in Sand Soil under Axial Load

**Ali Mohammed Basha**[a]

[a]*Dept. of Civil Engineering, Faculty of Engineering, Kafr El Sheikh University, Kafr El Sheikh 33511, Egypt*

**ARTICLE HISTORY**

Received 15 February 2019
Revised 1st 1 May 2019
Revised 2nd 3 May 2020
Accepted 7 June 2020
Published Online 18 January 2021

**KEYWORDS**

Slender pile
Vertical settlement
Lateral displacement
Post buckling
Partially embedded pile

**ABSTRACT**

Pile instability due to buckling is considered to be one of the most important causes of superstructures failures especially in bridges and wind turbines. The mechanism of load-transfer of partially embedded piles in sand subjected to axial load to surrounded soil and the corresponding deformation are important aspects of pile design. In the present research, an experimental model was developed to measure the lateral displacement of piles subjected to axial loads. The experimental results indicated that the post buckling load of partially embedded pile was enhanced up to five times of the buckling load of free case. Two proposed formulas based on the laboratory experiments were induced to determine post buckling load of the partially embedded pile. The predicted buckling capacity of piles was compared to the experimental buckling load, which showed a good agreement.

## 1. Introduction

Piles are slender structural elements that used to transfer the supper-structure loads to strong deeper layers whereas they tension or compression loads. Because a pile is often considered a slender element, it is in danger of buckling especially in the case of partially embedded pile. Slender piles are applied to many structures on shore such as bridges, offshore structures such as wind turbines and, platforms. Critical elastic buckling load of pile is considered as the maximum load which a pile can carry while staying straight without permanent deformation. On the other hand the post buckling load is the maximum load which a pile can bear at failure with permanent deformation. Many researchers investigated elastic buckling behavior of partially embedded piles. Where, the elastic buckling load can be defined as the maximum load which a pile can carry without any permanent deformation (staying straight). On the other hand, post buckling load can be defined as the maximum load which a pile can carry with permanent deformation (Avent and Alawady, 2005; Khodair and Hassiotis, 2006; Azizinamini et al., 2016; Azzam and Basha, 2018; Basha and Azzam, 2018; Salama and Basha, 2019).

Applying vertical loads at the top of the pile, vertical displacement take place and of the same time the pile bends laterally in any case of even small imperfection and produces lateral displacement. As the vertical pile load increased, the vertical displacement and the lateral displacement increased too until the pile reaches the failure condition. As the lateral displacement increased, the internal straining stress (action) changed from axially load to small eccentric compression and further to large eccentric compression at failure. There are two failure cases regarding the pile cross section by tension failure and the compression failure as stated by Chen et al. (2017). There are other causes for the failure of a partially embedded pile, and they were divided into three types; 1) failure of the bearing strata, 2) yielding of the pile cross section, 3) buckling failure, as stated by Vogt et al. (2009). Buckling failure is the most common cause of failure of partially embedded pile. There are many factors that affect the pile capacity and bucking length e.g., the total length L of pile, un-embedded (free length of piles ($L_{un}$), embedded length of piles ($L_{em}$), flexural rigidity of piles and the nonlinear support of soil (Lu and Zhao, 2017).

El Kamash and El Naggar (2018) investigated buckling behavior of end-bearing piles embedded on soft soil under axial load by

**CORRESPONDENCE** Ali Mohammed Basha ealibasha@yahoo.com Dept. of Civil Engineering, Faculty of Engineering, Kafr El Sheikh University, Kafr El Sheikh 33511, Egypt

applying the finite difference method. The numerical result showed that the buckling behavior significantly affect by the flexural stiffness of the pile as it increase the buckling load increase.

Few researches have been conducted to investigate the load–displacement curve of slender piles after the buckling process. Therefore in the current paper, the post-buckling behavior of the partially embedded pile in sand (coehesionless soil) was investigated experimentally. Effects of soil relative density and the slenderness of the pile were also considered for the post buckling analysis of the model type piles at different embedded lengths. The present paper focuses on the maximum lateral displacement, the p-y curve and the critical post buckling load.

## 2. Experimental Work

### 2.1 Set-Up Details

Figure 1 presents a sketch diagram which shows the experimental set-up considered in the current paper. The set up used to model a single pile subjected to axial compression. The main objective is present an experimental model well describe the behavior of a single pile under various partially embedded pile length ratio at different relative densities. The set-up consists of a cylindrical container made of stainless steel with inner diameter of 315 mm and a height equal to 850 mm. The cylindrical cell was supported on a base plate. A base plate supports the cylindrical container. Four steel rods form a loading frame as shown in Fig. 1 and tie the base and top plate together. This setup is similar to the one of Vogt et al. (2009) that examined the buckling of model type piles in soft clay.

### 2.2 Properties of Piles

A steel bars was used to model the pile. The embedment length of the modeled pile was $L_{em}$ and the unsupported length of the modeled pile was $L_{un}$ as illustrated in Fig. 1. The tested steel model piles had an outside diameters of $D$ = 8 mm, 10 mm and 12 mm. The tested piles had a total length equal to 1,200 mm with a slenderness ratios of ($L/D$ = 100, 120, and 150). The bars are made of normal mild and of high tensile steel. The steel bar nominal diameters were 8 mm, 10 mm and 12 mm. Both of the 10 mm bar and the 12 mm bar were of a high tensile steel (HTS) type, where the 8 mm bar was of a normal mild steel (NMS) type. Uniaxial tensile tests were carried out to determine the mechanical properties of the used steel bars. The yield strength and ultimate strength of NMS were 250 MPa and 344 MPa respectively. The yield strength and ultimate strength of HTS were 446.8 MPa and 538.5 MPa respectively. The modulus of elasticity was 200 GPa for all bars. The two ends of a modeled pile were considered as hinge.

### 2.3 Pile Installation Method

The installation method used in the current study can be described by the term of non-displacement or undisturbed. In this method, the model pile was mounted vertically at center of the test tank. Then the sand soil was poured uniformly on layers to attain the target relative densities as stated by Azzam and Mesmary (2010), Basha and Azzam (2018).

### 2.4 Soil Preparation and Characterization

Dry clean silica sand was used in this study (ASTM D422-63,

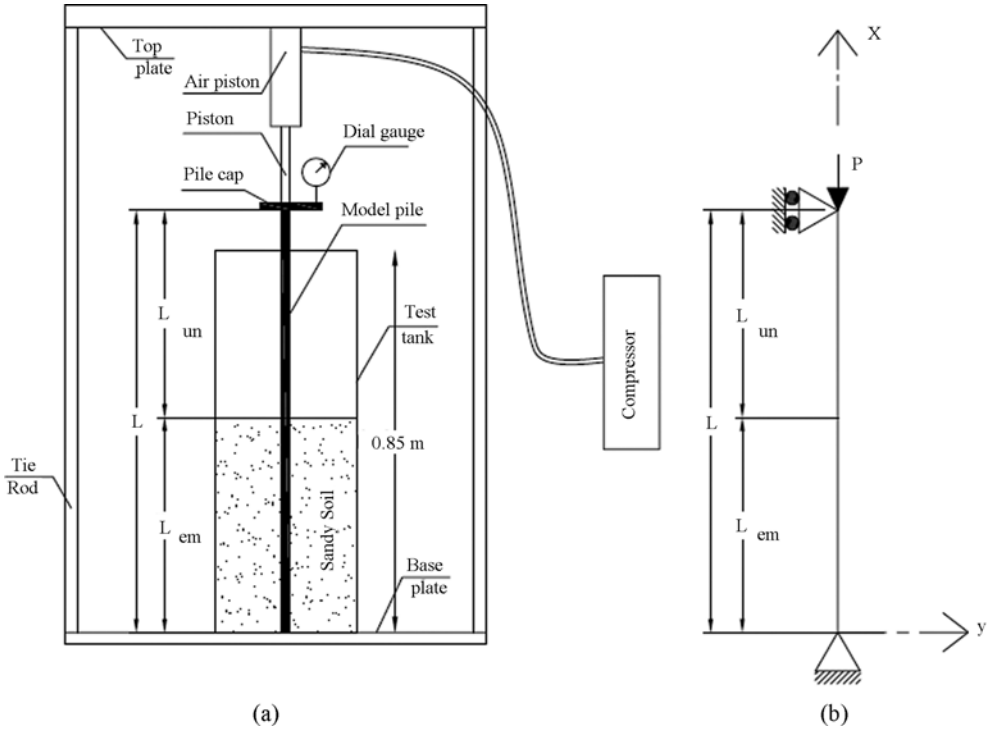


**Fig. 1.** Experimental Setup: (a) Schematic Diagram for the Test Setup, (b) The Static System of the Pile

**Table 1.** Geotechnical Properties of Sand Used in the Tests

| Property | Value |
|---|---|
| Effective grain size, $D_{10}$ (mm) | 0.26 |
| Average grain size, $D_{30}$ (mm) | 0.41 |
| Average grain size, $D_{60}$ (mm) | 0.61 |
| Uniformity coefficient, $C_u$ | 2.46 |
| Coefficient of curvature, $C_c$ | 1.02 |
| Maximum dry unit weight, $\gamma_d$ max (kN/m$^3$) | 18.75 |
| Minimum dry unit weight, $\gamma_d$ min (kN/m$^3$) | 16.82 |
| Maximum void ratio, $e_{max}$ | 0.565 |
| Minimum void ratio, $e_{min}$ | 0.392 |
| Specific gravity, $G_s$ | 2.65 |
| Coarse sand (%) | 30 |
| Medium sand (%) | 62 |
| Fine sand (%) | 8 |
| Peak angle of internal friction at $D_r$ = 50% (°) | 30 |
| Peak angle of internal friction at $D_r$ = 65% (°) | 35 |
| Peak angle of internal friction at $D_r$ = 85% (°) | 38 |

2007). The shear parameters were determined experimentally by direct shear box apparatus at a relative density of $D_r$ of 50%, 65% and 85% (ASTM D3080/D3080M-11). The soil used had an effective particle size ($D_{10}$) equals to 0.26 mm, a uniformity coefficient ($C_u$) equals to 2.46 and a coefficient of curvature ($C_c$) equals to 1.02. The target relative density was obtained by compact the purred sand manually by applying hammer with weight 30 N until reaching the required relative density. Table 1 lists the properties of the used soil.

## 3. Test Program and Parameters

Seventy-five tests were conducted on the model pile to investigate the effect of the unsupported length $L_{un}/L$ and embedded length $L_{em}/L$ of the pile, the pile slenderness ratio $L/D$ and the soil relative density on the pile post buckling load. The tested piles were categorized using three groups based on the relative density and the pile diameter. Table 2 shows a summary of the test parameters test and the corresponding test result.

### 3.1 Test Procedure

The buckling tests were conducted using a monotonically increasing axial load. Fig. 1 shows the test setup. The vertical loads were stepwise applied to the pile through a vertical piston connected to the head of the pile with pin end. The vertical piston was centrically mounted on top of the pile head. The vertical piston was connected to an air compressor which used to increase the applied pressure. Each load step was kept constant for 5 minutes. Horizontal dial gauges were used to measure lateral displacement at the pile middle.

## 4. Results and Discussions

The axial load, vertical displacement of the pile head and the lateral displacement of the pile shaft were recorded. Table 3 presents the post buckling loads and the corresponding maximum lateral displacement at different ratios of partially embedded length $L_{em}/L$ and $L_{un}/L$, respectively. The curves of the lateral displacement along the pile length for various embedded length ratios are drawn in Figs. 2, 3 and 4. The bearing behavior of the partially embedded pile was studied using lateral displacement curves (p-y curve).

### 4.1 Lateral Displacement along the Pile

Figures 2, 3 and 4 show the lateral displacement along the pile length for $L/D$ = 100, 120 and 150. The lateral displacement of the pile is higher at the unsupported section and the maximum lateral displacement is for all cases rather close to the ground surface. Furthermore, all the tested piles show that the maximum lateral displacement occurred above the ground level.

Figure 2 shows the measured lateral displacement of the pile at different embedded length ratios for three relative densities of the sand. The minimum lateral displacement at post buckling was registered for case of the unsupported pile ($L_{em}$ = zero) and the lateral displacement curve was almost symmetric with its axis about the pile middle. The maximum lateral displacement at post buckling took place at an embedded length ratio equal to 0.50. The general trend of the lateral displacement increased as the embedded length percentage increased to 50%. Then its value decreased with increasing the embedded length percentage, as shown in Figs. 3 and 4.

As the axial load was increased, the pile gradually displaced laterally till it reached the buckling load, then the pile moved laterally, in dramatically way, to reach the maximum lateral displacement suddenly. The induced lateral deformation shape was a curve that was small at the upper and the lower third and large in the middle third. As a general trend, the deformation at the unsupported part of the pile was much larger than that at the embedded part of the pile which was supported laterally by the

**Table 2.** Model Tests Program

| Group | Pile diameter ($d$ mm) | Relative density ($D_r$ %) | Unsupported pile length ($L_{un}$ mm) | Embedded pile length ($L_{em}$ mm) | Installation method |
|---|---|---|---|---|---|
| I | 8 | 50%, 65% and 85% | 400, 500, 600, 700, 800, 900, 1,000, 1,100 and 1,200 | 0.0, 100, 200, 300, 400, 500, 600, 700 and 800 | Non-displacement method |
| II | 10 | | | | |
| II | 12 | | | | |

**Table 3.** Post Buckling Load of Pile at Different Studied Parameters

| Group | Pile number | $L_{em}/L$ | $L_{un}/L$ | Post buckling load and max. lateral buckling | | | | | |
|---|---|---|---|---|---|---|---|---|---|
| | | | | $D_r$ = 50% | | $D_r$ = 65% | | $D_r$ = 85% | |
| | | | | $P_{cr}$ N | $\delta_{H\text{-}max}$ mm | $P_{cr}$ N | $\delta_{H\text{-}max}$ mm | $P_{cr}$ N | $\delta_{H\text{-}max}$ mm |
| I | $P_{I}$ | Zero | 1 | 279 | 30 | 279 | 30 | 279 | 30 |
| | $P_{I\text{-}1}$ | 1/12 | 11/12 | 355 | 37 | 370 | 38 | 390 | 35 |
| | $P_{I\text{-}2}$ | 1/6 | 5/6 | 430 | 44 | 460 | 43 | 550 | 44 |
| | $P_{I\text{-}3}$ | 1/4 | 3/4 | 510 | 52 | 580 | 49 | 687 | 54 |
| | $P_{I\text{-}4}$ | 1/3 | 2/3 | 590 | 60 | 690 | 57 | 825 | 55 |
| | $P_{I\text{-}5}$ | 5/12 | 7/12 | 710 | 59 | 860 | 58 | 985 | 67 |
| | $P_{I\text{-}6}$ | 1/2 | 1/2 | 820 | 64 | 1,000 | 65 | 1,180 | 72 |
| | $P_{I\text{-}7}$ | 7/12 | 5/12 | 945 | 65 | 1,180 | 58 | 1,415 | 65 |
| | $P_{I\text{-}8}$ | 2/3 | 1/3 | 980 | 66 | 1,260 | 56 | 1,530 | 67 |
| | $P_{II}$ | zero | 1 | 785 | 44 | 785 | 44 | 785 | 44 |
| II | $P_{II\text{-}1}$ | 1/12 | 11/12 | 982 | 57 | 1,050 | 57 | 1,130 | 57 |
| | $P_{II\text{-}2}$ | 1/6 | 5/6 | 1,180 | 66 | 1,400 | 66 | 1,845 | 65 |
| | $P_{II\text{-}3}$ | 1/4 | 3/4 | 1,425 | 70 | 1,700 | 73 | 1,965 | 80 |
| | $P_{II\text{-}4}$ | 1/3 | 2/3 | 1,720 | 89 | 2,030 | 85 | 2,360 | 84 |
| | $P_{II\text{-}5}$ | 5/12 | 7/12 | 2,120 | 90 | 2,370 | 85 | 2,650 | 102 |
| | $P_{II\text{-}6}$ | 1/2 | 1/2 | 2,278 | 103 | 2,800 | 100 | 3,340 | 102 |
| | $P_{II\text{-}7}$ | 7/12 | 5/12 | 2,555 | 90 | 3,150 | 90 | 3,730 | 95 |
| | $P_{II\text{-}8}$ | 2/3 | 1/3 | 2,750 | 96 | 3,350 | 86 | 3,930 | 94 |
| III | $P_{III}$ | zero | 1 | 1,610 | 62 | 1,610 | 62 | 1,610 | 62 |
| | $P_{III\text{-}1}$ | 1/12 | 11/12 | 1,965 | 75 | 1,965 | 75 | 1,965 | 85 |
| | $P_{III\text{-}2}$ | 1/6 | 5/6 | 2,360 | 94 | 2,450 | 94 | 2,555 | 85 |
| | $P_{III\text{-}3}$ | 1/4 | 3/4 | 3,140 | 98 | 3,350 | 98 | 3,535 | 92 |
| | $P_{III\text{-}4}$ | 1/3 | 2/3 | 3,535 | 84 | 3,800 | 102 | 4,125 | 104 |
| | $P_{III\text{-}5}$ | 5/12 | 7/12 | 3,930 | 106 | 4,350 | 109 | 4,715 | 110 |
| | $P_{III\text{-}6}$ | 1/2 | 1/2 | 4,520 | 115 | 5,000 | 115 | 5,500 | 104 |
| | $P_{III\text{-}7}$ | 7/12 | 5/12 | 5,500 | 141 | 5,800 | 118 | 6,480 | 107 |
| | $P_{III\text{-}8}$ | 2/3 | 1/3 | 6,285 | 127 | 7,070 | 106 | 7,465 | 107 |

sand.

It can be concluded based on the experimental result that an increase of the embedded pile length usually affects the bearing capacity of the pile by increasing the post buckling load and reduce the lateral deformation. In all cases the deformation of the unsupported part of the pile is larger than the supported part. The embedded part of the pile was only marginally affected. The pile carries axial load and deforms inside the soil where the soil gives a certain confinement. The shape of the buckling pile is consistent with the analytical solution stated earlier by Gabr et al. (1994, 1997) for pinned-pinned condition.

## 4.2 Effect of the Unsupported Length on the Post Buckling Load

The effect of the unsupported length on the post buckling load for different slenderness ratios of 100, 120 and 150 and different relative densities of 50%, 65% and 85% are presented in Fig 5. The soil relative density had an insignificant effect on the final value of the post buckling load when the normalized unsupported length ($L_{un}/L$) ranged between 0.90 to 1.0. The increase in the post buckling load due the increase in the relative density from 50% to 85% were about 50%, 40% and 16% for the slenderness ratios of 150, 120 and 100 respectively at a normalized unsupported length equal to 1/3. By taking the value of the post buckling load for the slenderness ratio equal to 150 as a reference; the increase in the post buckling load reached about 250% and 450% for the slenderness ratios of 120 and 100, respectively. The increase in the post buckling load reached about 270% and 520% for the slenderness ratio 120 and 100, respectively. The increase of the post buckling load reaches about 280% and 620% for the slenderness ratio 120 and 100, respectively. The variation of the post buckling load with respect to the normalized unsupported length was approximately linear and reversal. This result is consistent with those stated by Lin et al. (2010) and Jesmani et al. (2014).

## 4.3 Effect of Soil Density on the Post Buckling Load

The behavior of the partially embedded piles was almost similar

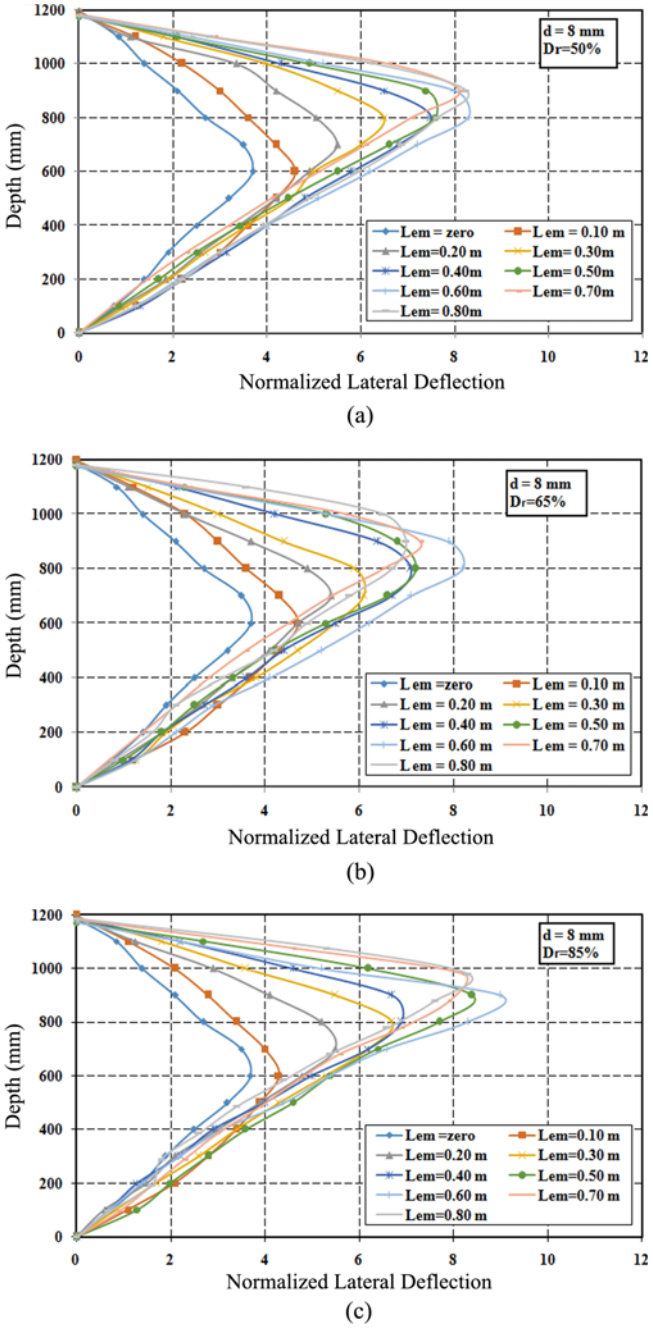


**Fig. 2.** Variation of Normalized Lateral Displacement versus Pile Depth at Different Embedded Length for $d$ = 8 mm: (a) Relative Density = 50%, (b) Relative Density = 65%, (c) Relative Density = 85%

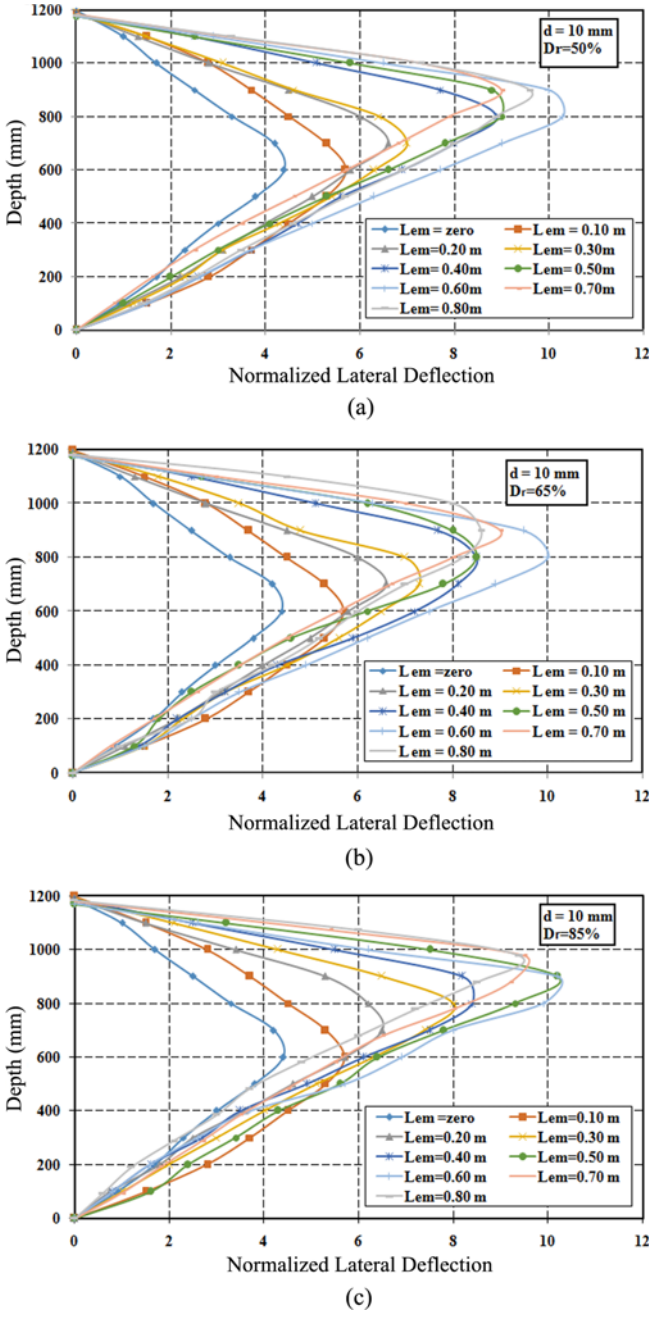


**Fig. 3.** Variation of Normalized Lateral Displacement versus Pile Depth at Different Embedded Length for $d$ = 10 mm: (a) Relative Density = 50%, (b) Relative Density = 65%, (c) Relative Density = 85%

in loose ($D_r$ = 50%), medium $D_r$ = 65%) as well as dense ($D_r$ = 85%) states of sand. The effect of the soil state (relative density) becomes insignificant as the pile flexural stiffness increases.

## 5. Theoretical Study

### 5.1 Evaluation of Buckling Coefficient of the Total Length

Euler's buckling load for the case of the unsupported pile $L_{un} = L$ can be expressed by the following equation:

$$P_E = \frac{\pi^2 EI}{L^2}. \tag{1}$$

Based on the experimental result, the post buckling load in the case of a partially supported pile is higher than Euler's load because of the stabilizing interaction between the pile and the surrounding soil. The critical post buckling load $P_{cr}$ for the axially loaded can be as well written in the following form:

$$P_{cr} = \frac{\pi^2 EI}{(\alpha L)^2}, \tag{2}$$

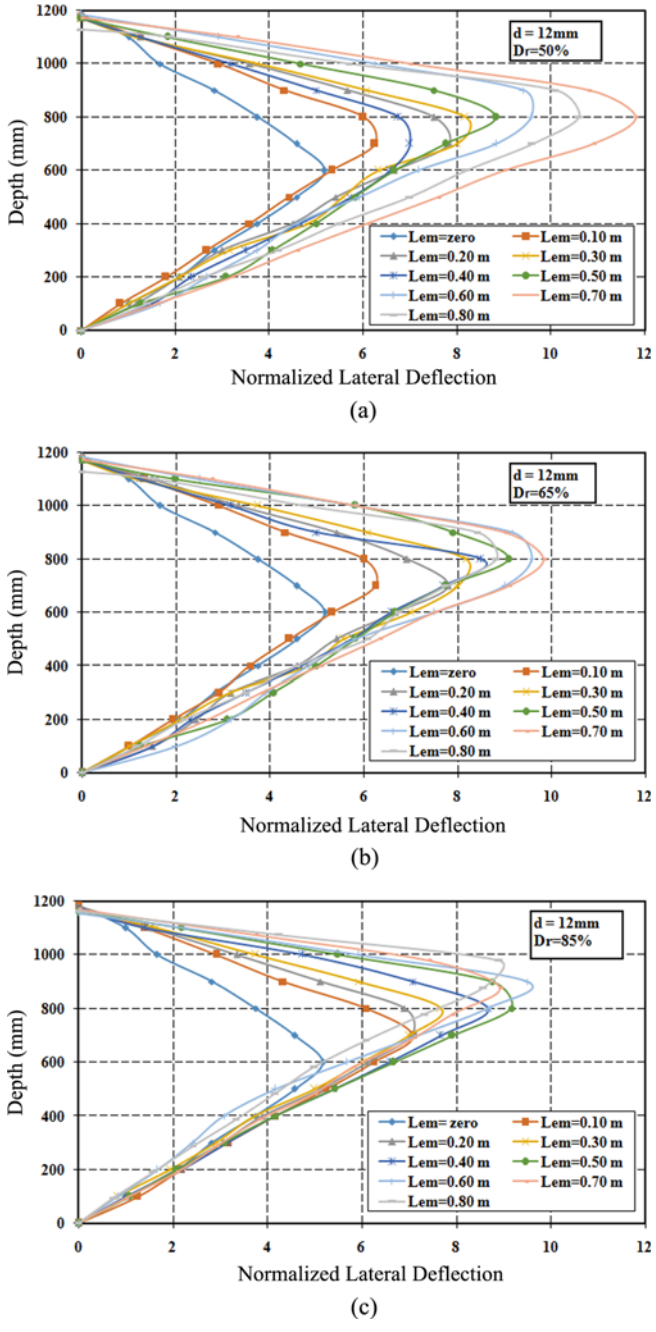


**Fig. 4.** Variation of Normalized Lateral Displacement versus Pile Depth at Different Embedded Length for $d$ = 12 mm: (a) Relative Density = 50%, (b) Relative Density = 65%, (c) Relative Density = 85%

where $L$ is the total pile length and $\alpha$ is a post buckling coefficient that defines the ratio between the effective buckling length and the total pile length.

Figures 6 to 8 present the variation of buckling coefficient $\alpha$ with the normalized embedded length $L_{em}/L$ for two important influencing parameters. First, one is the slenderness ratio which equals 100, 120 and 150 for the examined model piles. Second, one is the relative density of the sand which was chosen of 50%, 65% and 85%. As a general trend; the relation between $\alpha$ and $L_{em}/L$ can be described by a power function. As the normalized

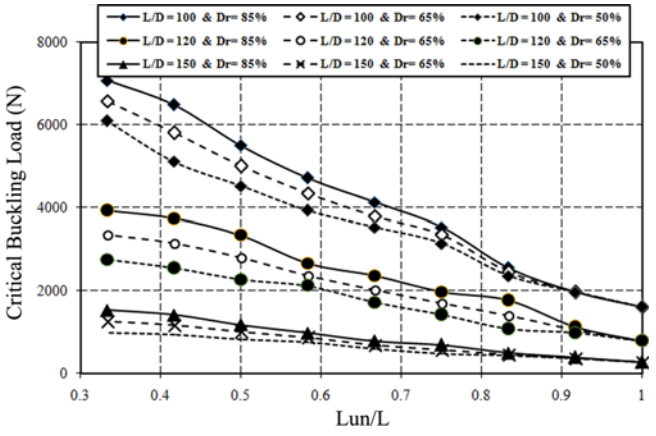


**Fig. 5.** Variation of Critical Buckling Load versus Normalized Length of Pile Partially Embedded In Different Granular Soils State

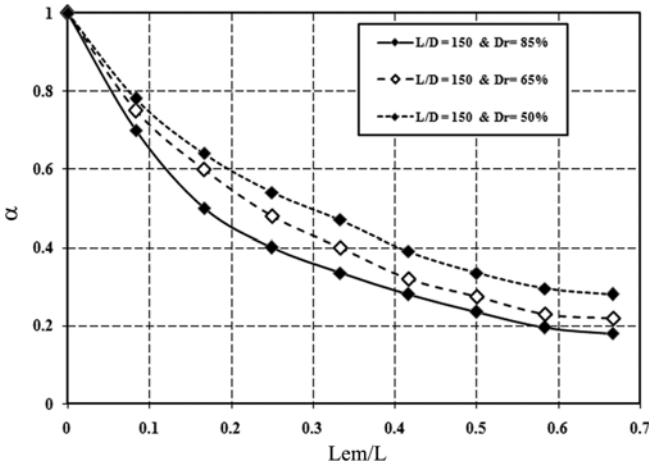


**Fig. 6.** Variation of Buckling Coefficient of Total Length versus Normalized Embedded Length of Pile in Different Granular Soils State for $d$ = 8 mm

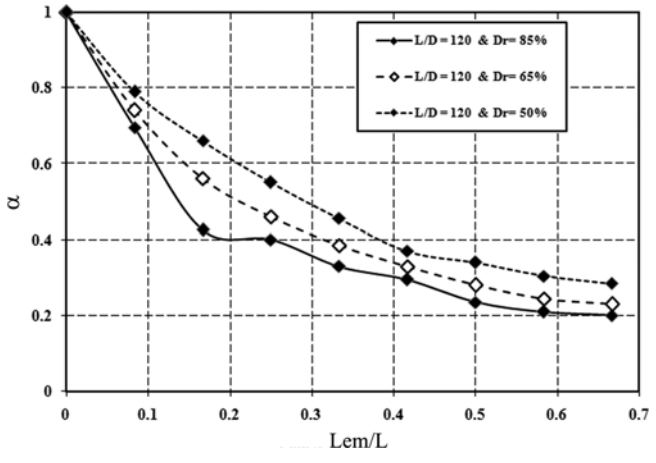


**Fig. 7.** Variation of Buckling Coefficient of Total Length versus Normalized Embedded Length of Pile in Different Granular Soils State for $d$ = 10 mm

embedded length increases the buckling coefficient of the total length decreases. That higher the relative density that faster the

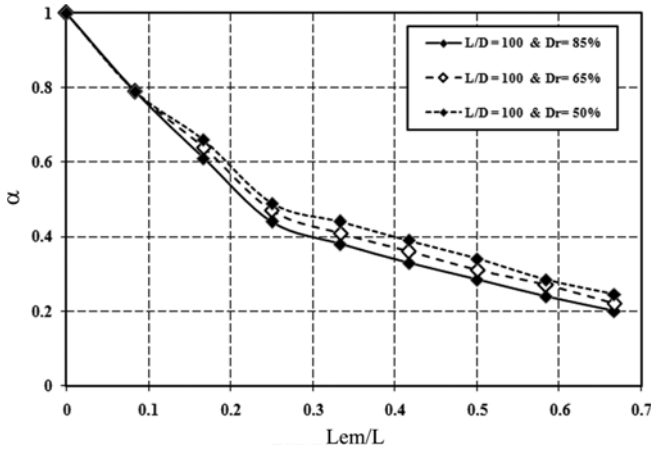


**Fig. 8.** Variation of Buckling Coefficient of Total Length versus Normalized Embedded Length of Pile in Different Granular Soils State for $d$ = 12 mm

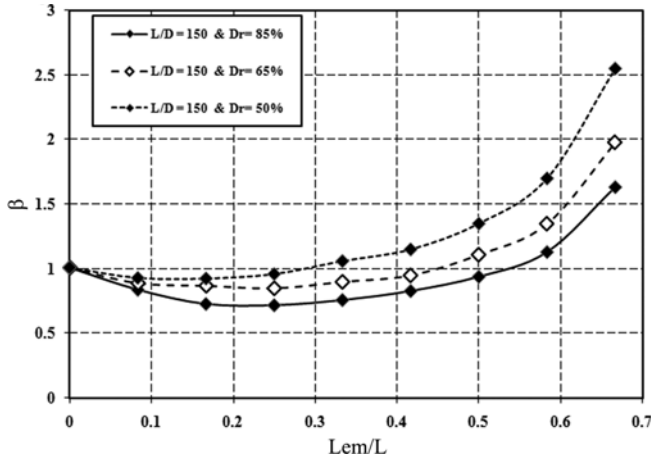


**Fig. 9.** Variation of Buckling Coefficient of Unsupported Length versus Normalized Embedded Length of Pile in Different Granular Soils State for $d$ = 8 mm

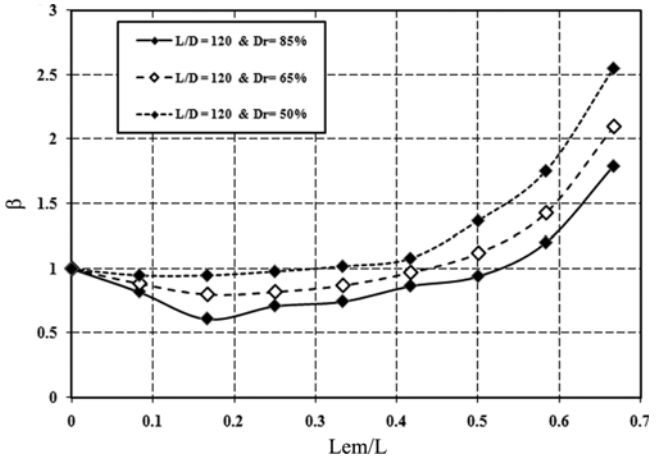


**Fig. 10.** Variation of Buckling Coefficient of Unsupported Length versus Normalized Embedded Length of Pile in Different Granular Soils State for $d$ = 10 mm

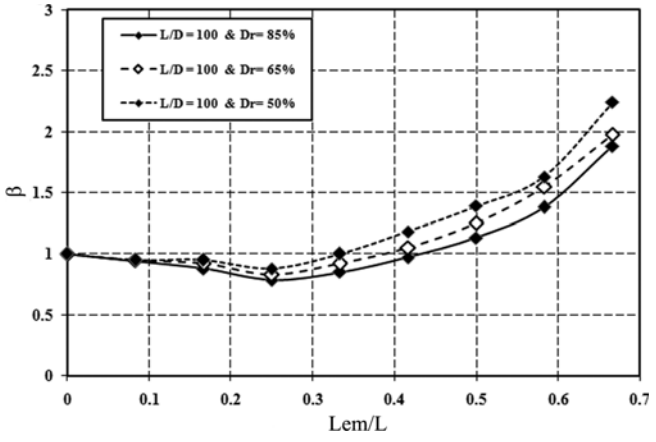


**Fig. 11.** Variation of Buckling Coefficient of Unsupported Length versus Normalized Embedded Length of Pile in Different Granular Soils State for $d$ = 12 mm

coefficient $\alpha$ decreases with increasing $L_{em}/L$. The average percentage of difference between the values of the buckling coefficient were about 7%, 16% and 18% for the slenderness ratio 100, 120 and 150, respectively, at the same relative of density. The average value of $\alpha$ coefficient was 0.46, 0.47 and 0.50 for the slenderness ratio 150, 120 and 100, respectively. The average value of $\alpha$ coefficient was about 0.475.

## 5.2 Evaluation of Buckling Coefficient of the Unsupported Length

Based on the experimental result, there were more increases in the critical post buckling load increases from the Euler's load load for the unsupported pile with increasing soil support governed by the interaction between the pile and the surrounding soil. The critical post buckling load $P_{cr}$ for the axially loaded pile can be written in the following form:

$$P_{cr} = \frac{\pi^2 EI}{(\beta L_{un})^2}, \tag{3}$$

where $L_{un}$ is the unsupported pile length and $\beta$ is a post buckling coefficient of the unsupported pile length that defined as the ratio of the effective post buckling length and the unsupported pile length.

Figures 9, 10 and 11 presents the variation of buckling coefficient of the unsupported length $\beta$ with the normalized embedded length $L_{em}/L$ considering the main governing parameters $L/D$ and $D_r$ which are used previously for analyzing the parameter $\alpha$. The relation between $\beta$ and $L_{em}/L$ is approximately a parabolic function. As the normalized embedded length increased the buckling coefficient of the unsupported length increases as well. That higher the relative density of the sand that smaller $\beta$ gets for all the examined $L/D$ ratios. Within the examined range of $L/L_{em}$ the differences between the values of the buckling coefficient $\beta$ were about 9%, 18% and 20% for the slenderness ratio 100, 120 and 150, respectively. The average value of the $\beta$ coefficient was 1.13, 1.14 and 1.18 for the slenderness ratio 150, 120 and 100, respectively. The average value of $\beta$ coefficient was about 1.15.

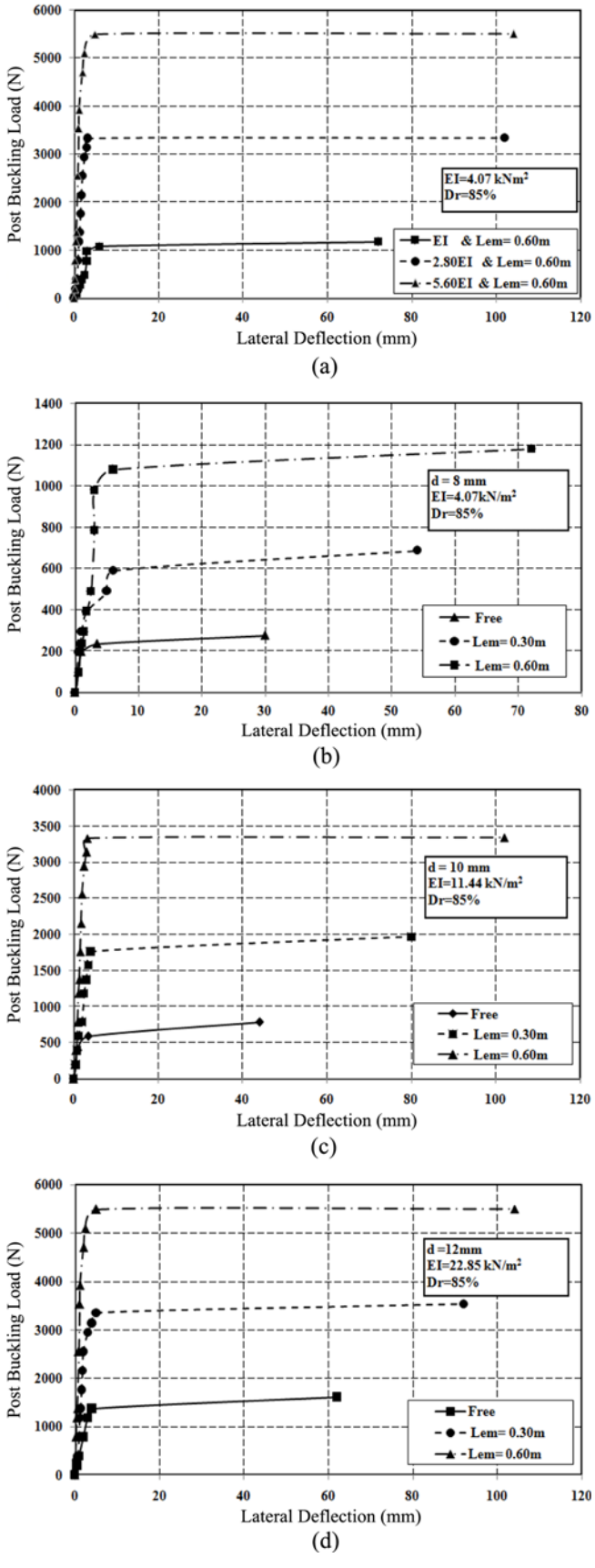


**Fig. 12.** P-y Curve at: (a) Different Flexural Stiffness, (b) $d$ = 8 mm & $D_r$ = 85%, (c) $d$ = 10 mm & $D_r$ = 85%, (d) $d$ = 12 mm & $D_r$ = 85%

## 6. Flexural Stiffness

The theoretical Euler's buckling load of the modeled pile tests was assumed to be the same as the measured values i.e., 279 N, 785 N and 1,567 N for pile diameters of 8 mm, 10 mm and 12 mm, respectively. Thus an effective flexural stiffness (EI) of the modeled pile was back-calculate based on the Euler's formula to take into account imperfection. The back calculated EI values were 4.07 kNm$^2$, 11.444 kNm$^2$ and 22.8 kNm$^2$ for pile diameters of 8 mm, 10 mm and 12 mm, respectively. According to the experimental results, the critical buckling load of the pile partially surrounded up to 2/3 of its length by soil, it was approximately five times of the corresponding unsupported case.

Figure 12 shows the load-lateral displacements for different flexural stiffnesses of the pile and varying embedded lengths for pined end conditions. The experimental results indicate that the flexural stiffness of the pile had a significant effect on the post buckling load. As the flexural pile stiffness increased from EI of the smallest model pile to 2.8 EI and 5.6 EI, the lateral displacement increased from 72 mm to 102 mm and 104 mm at buckling; also the critical post buckling load increased from 1,180 N to 3,340 N and 5,500 N, respectively. The relative increase of the critical post buckling load reached 4.66 because of the change of the flexural stiffness of the pile from EI to 5.6 EI, as shown in Fig. 12(a).

Figures 12(b), 12(c) and 12(d) present the lateral displacement versus the post buckling load at different embedded lengths. The general trend of lateral displacement; it changes linearly until the pile load reaches the post buckling load. After loss of stability the displacements increases significantly.

For piles with a diameter of 8 mm at relative density equal to 85%, the critical post buckling load increased from 275 N to 687 N and 1,180 N for the embedded pile length ratios of zero, 0.25 and 0.50, respectively as shown in Fig. 12(b). For piles with a diameter of 10 mm at a relative density equal to 85%, the critical post buckling load increased from 785 N to 1,965 N and 3,340 N for embedded pile length ratios zero, 0.25 and 0.50, respectively as shown in Fig. 12(c). For piles with a diameter of 12 mm at a relative density equal to 85%, the critical post buckling load increased from 1,610 N to 3,535 N and 5,500 N for the embedded pile length ratio of zero, 0.25 and 0.50, respectively as shown in Fig. 12(d).

## 7. Comparison with Experimental Results

To apply the proposed simplified Eqs. (2) and (3) that generalize the buckling length considering the embedded pile length a comparison with other well documented laboratory tests reported by Lee (1968) and Gouvenot (1975) was done. Heelis et al in 2004 derives an analytical formula using for predicting the buckling load of partially bedded piles. The results of this analytical formula applied on the parameters of the tests by Lee (1968) and Gouvenot (1975) were compared to the test results presented in this study. The differences between the calculated values of $\alpha$ and $\beta$ from the tests of Lee (1968) and Gouvenot (1975) and the $\alpha$ and $\beta$ values from the present experimental study are presented

**Table 4.** Theoretical Values Compared with Lee's and Gouvenot's Experimental Buckling Loads

| Reference | Soil type | Pile type | Flexural stiffness (EI) $Nmm^2 \times 10^6$ | Total pile length (L) mm | Embedded pile length ($L_{un}$) mm | Buckling load: N | | | | |
|---|---|---|---|---|---|---|---|---|---|---|
| | | | | | | Experiment | $\alpha$ formula | % Diff. | $\beta$ formula | % Diff. |
| Lee, 1968 | Medium loose sand | Aluminum tube | 8.47 | 1,630 | 840 | 222 | 142.58 | 35.77 | 103 | 53.55 |
| | Dense sand | Steel rod | 67.2 | 1,580 | 840 | 1,245 | 1,203.7 | 3.32 | 818 | 34.0 |
| Gouvenot, 1975 | Peat | Concrete piles | 8,000 | 4,000 | 4,000 | 20,000 | 21,889 | 9.45 | 4,294 | 78.5 |
| | Soft clay | | | | | 40,000 | 21,889 | 9.45 | 4,294 | 78.5 |

in Table 4. Table 4 as well summarizes the dimensions and properties of examined model piles and compare the experimentally found buckling loads with two proposed formulas.

The theoretical buckling load by Heelis et al. (2004) calculated at the given parameters $L/L_{em}$, EI and Dr from the tests of Lee (1968) and Gouvenot (1975) is considerably higher compared to the test results presented in this study. The general trend of the $\alpha$ formula and the $\beta$ formula results to be a considerable underestimate of the experimental buckling load. The formula based on the total pile length gives a more accurate result than the formula based on the embedded pile length.

## 8. Failure Mechanisms

The pile transfers its loads to the surrounded soil by two main methods, first one is the shaft friction and second one is the base resistance. When applying load to the pile head, it deform mainly in the vertical direction and the surrounding soil offers shaft resistance to the downward movement. Because soil is a frictional material, frictional forces develop at the interface at the pile shaft and the surrounding soil that opposes the downward pile movement. The frictional forces acting all along the pile shaft partly resist the applied axial load and are referred to as shaft resistance, shaft friction or skin friction. Another part of the axial load is transferred to the soil through the pile tip (base resistance).

Figure 13 presents a simplified static system of the soil-pile interaction along the pile length during the buckling. Fig. 13(a) shows the load transfer mechanism of the partially embedded pile under the axial load. Fig. 13(b) shows a sketch of the lateral displacement for a buckling pile. Fig. 13(c) illustrates the distribution

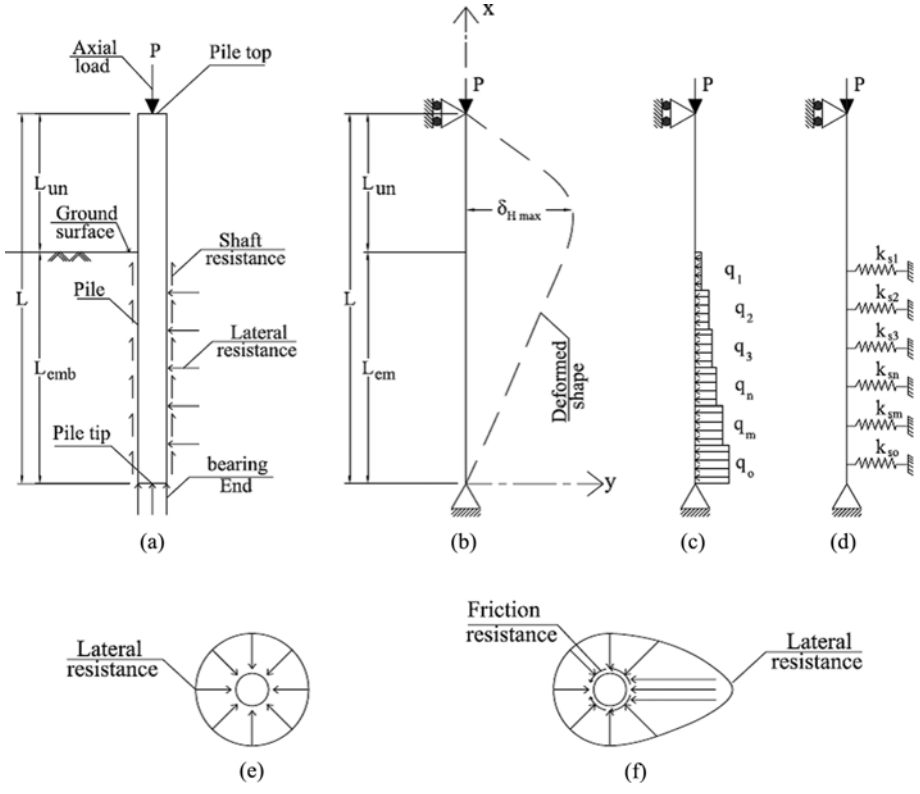


**Fig. 13.** Distribution of Soil-Pile Reaction along Pile Length: (a) Load Transfer Mechanism of Partially Embedded Pile under Axial Load Piles during Buckling, (b) Pile Lateral Displacement Pattern, (c) Soil Reaction Distribution along Pile Length, (d) Soil-Pile Modeling, (e) Stresses on a Pile before Buckling, (f) Stresses on a Pile during Buckling

of the soil support along pile length based on the pile-lateral displacement. The stiffness of the soil support decreases as the deformation increases (see p-y curves). Fig. 13(d) shows the proposed static model representing soil- pile system based on the Winkler method. The soil stiffness is simplified by a spring. The stiffness of the spring decreases as the deformation increases. At the failure of the soil where the ultimate shear strength is reached the stiffness of the spring is zero. Stress distribution along the pile perimeter at rest (before loading) is uniform along the pile circumference and it increases with the soil depth as presented in Fig. 13(e). During the loading process, the pile start to bend until it reaches the post buckling failure. The resultant of the stresses distribution along the pile perimeter becomes non-uniform as illustrated in Fig. 13(f).

Based on the bearing mechanism illustrated in Fig. 13, the pile end condition at the tip or base is restrained by two main parameters of relative stiffness for the soil-pile system and the slenderness ratio for the pile. For short piles, the tip end condition may be considered as a hinge. While for the long pile, the tip end condition may be considered as a fixed. The top pile condition can be modelled as one of a hinged, fixed or free end depending on the connection to the superstructure. A hinged end can be considered for pile supporting bridges or surface structures. A fixed end can be considered for piles supporting high rise building or massive foundation. A free end can be considered for piles used as retaining structures.

## 9. Conclusions

Based on the test results the following conclusions can be obtained:

1. The change of the embedded length of the pile is affected by the pile lateral displacement especially at the pile upper part. In general, the buckling length increases during loading because of soil failure at the surface.
2. For the examined test conditions the increase of the buckling resistance of embedded piles is as much as 500% compared to the corresponding unsupported pile.
3. The average value of the buckling coefficient of the unsupported pile length is about 1.15.
4. The average value of buckling coefficient of the total length pile length is about 0.475.
5. The flexural stiffness and imperfection of piles may be considered as the main parameters affecting the buckling load.
6. Within the range of the examined tests conditions, the unsupported pile length as well the ratio between the free length and the embedded length have a great effect on the buckling load.
7. A large number of tests were carried out at 3 different relative densities of the sand supporting the pile shaft, 3 different model piles with varying flexural stiffness and slenderness respectively were examined. Moreover, different ratios of total pile length and embedded pile length were analyzed by experiments. Hence, the test data provides the possibility to excessively verify analytical, empirical or numerical models predicting the buckling load of piles.

## Acknowledgments

Not Applicable

## ORCID

Not Applicable

## References

ASTM D422-63 (2007) Testing and materials specifications. ASTM D422-63, ASTM International, West Conshohocken, PA, USA

Avent RR, Alawady M (2005) Bridge scour and substructure deterioration: Case study. *Journal of Bridge Engineering* 10(3):247-254, DOI: 10.1061/(asce)1084-0702(2005)10:3(247)

Azizinamini A, Yakel A, Sherafati A, Taghinezhad R, Gull JH (2016) Flexible pile head in jointless bridges: Design provisions for H-piles in cohesive soils. *Journal of Bridge Engineering* 21(3):04015064, DOI: 10.1061/(asce)be.1943-5592.0000791

Azzam WR, Al Mesmary M (2010) The behavior of single subjected to surcharge loading. *NED University Journal of Research* VII (1):1012

Azzam WR, Basha AM (2018) Utilization of micro-piles for improving the sub-grade under the existing strip foundation: Experimental and numerical study. *Innovative Infrastructure Solutions* 3(1), DOI: 10.1007/s41062-018-0149-0

Basha A, Azzam WR (2018) Uplift capacity of single pile embedded in partially submerged sand. *KSCE Journal of Civil Engineering* 22(12):4882-4890, DOI: 10.1007/s12205-017-1715-2

Chen L, Chen Y, Shi J, Chen G (2017) Small- and large-scale model tests on the buckling property of slender pile. *Marine Georesources & Geotechnology* 35(8):1058-1067, DOI: 10.1080/1064119X.2017.1285378

El Kamash W, El Naggar H (2018) Numerical study on buckling of end-bearing piles in soft soil subjected to axial loads. *Geotechnical and Geological Engineering* 36:3183-3201, DOI: 10.1007/s10706-018-0529-4

Gabr MA, Wang J, Kiger SA (1994) Effect of boundary conditions on buckling of friction piles. *Journal of Engineering Mechanics* 120(6):1392-1400, DOI: 10.1061/(ASCE)0733-9399(1994)120:6(1392)

Gabr MA, Wang JJ, Zhao M (1997) Buckling of piles with general power distribution of lateral subgrade reaction. *Journal of Geotechnical and Geoenvironmental Engineering* 123(2):123-130, DOI: 10.1061/(ASCE)1090-0241(1997)123:2(123)

Gouvenot D (1975) Essais de chargement et de flambement de pieux aiguilles. *Annales de l'Institut Technique du Batiment et des Travaux Publics* 334:25-39

Heelis ME, Pavlović MN, West RP (2004) The analytical prediction of the buckling loads of fully and partially embedded piles. *Géotechnique* 54(6):363-373, DOI: 10.1680/geot.2004.54.6.363

Jesmani M, Nabavi SH, Kamalzare M (2014) Numerical analysis of buckling behavior of concrete piles under axial load embedded in sand. *Arabian Journal for Science and Engineering* 39(4):2683-2693, DOI: 10.1007/s13369-014-0970-5

Khodair Y, Hassiotis S (2006) Buckling behaviour of single pile and pile bent in the Scotch Road Bridge. *Geomechanics and Geoengineering* 1(4):291-298, DOI: 10.1080/17486020600834621

Lee KL (1968) Buckling of partially embedded piles in sands. *Journal of the Soil Mechanics and Foundations Division* 94(1):255-270

Lin C, Bennett C, Han J, Parsons RL (2010) p-y based approach for buckling analysis of axially loaded piles under scoured conditions. Structures congress 2010, May 12-15, Orlando, FL, USA, DOI: 10.1061/41130(369)12

Lu W, Zhao D (2017) Analysis on calculated length for buckling stability of steel pipe pile based on energy method. *The Open Civil Engineering Journal* 11:167-175, DOI: 10.2174/1874149501711010167

Salama MI, Basha AM (2019) Elastic buckling loads of partially embedded piles in cohesive soil. *Innovative Infrastructure Solutions* 4(1), DOI: 10.1007/s41062-019-0198-z

Vogt N, Vogt S, Kellner C (2009) Buckling of slender piles in soft soils. *Bautechnik* 86(S1):98-112, DOI: 10.1002/bate.200910046